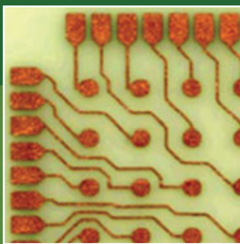

Epitaxial PZT films for MEMS printing applications

Hiroshi Funakubo, Matthijn Dekkers, Alessia Sambri, Stefano Gariglio, Igor Shklyarevskiy, and Guus Rijnders

Films of piezoelectric and ferroelectric oxides have been widely investigated for various applications, including microelectromechanical systems (MEMS) for printing. $Pb(Zr,Ti)O_3$ is of particular interest due to its excellent piezoelectric properties. Control of the density, crystalline orientation, and compositional uniformity is essential to obtain these properties. In this article, we review recent progress on the fabrication of epitaxial $Pb(Zr,Ti)O_3$ films, in which the aforementioned control can be achieved. We discuss the different approaches used for the deposition of the epitaxial piezoelectric layer as well as the achieved degrees of the epitaxy. Furthermore, the integration of these piezoelectric layers in MEMS and the corresponding performance are discussed.

Introduction to piezo MEMS printing

This article covers recent progress on the fabrication of epitaxial piezoelectric thin films. The crystalline quality of these epitaxial thin films is such that optimal piezoelectric properties with long-term stability can be obtained. This is important for many piezoelectric applications, such as piezoelectric inkjet printing. Inkjet print heads represented 15% of a US$10 billion microelectromechanical systems (MEMS) market in 2011.[1] While thermal print heads, mostly for small office/home office (SOHO), have currently the major share of the MEMS inkjet market because they enable complementary metal oxide semiconductor compatible manufacturing, piezoelectric print heads are an emerging product in the professional printing arena. When comparing the two printing (droplet generation, see **Figure 1**) principles—thermal versus piezoelectric—the major advantage of the former, which is often decisive for the final product, is an extremely low price-per-nozzle combined with very high integration density (high dot-per-inch resolution). This makes thermal inkjet (TIJ) devices with throwaway print heads very attractive for SOHO and the low-end professional printing markets. However, thermal inkjets impose very stringent demands on the ink due to the fundamental limitation of the droplet formation process, which requires explosive liquid evaporation to create pressure in the print head for ink ejection. Therefore, TIJ print heads can only operate with water-based inks with a rather limited viscosity and temperature range.

In contrast, the piezoelectric inkjet (PIJ) (see Figure 1b), which utilizes pure mechanical pressure created by the piezoelectric element, though more expensive, is able to jet a wide range of fluids over an extended temperature region. This universality makes PIJ an attractive tool not only for the high-end professional market, but also paves the way for industrial printing (e.g., electronics, 3D prototyping, bio- and medical printing) (see **Figure 2**). Additionally, PIJ print heads are more reliable and robust due to the possibility of early nozzle failure detection by using the piezoelectric actuator as a sensor while idle.[2,3]

As mentioned previously, the disadvantage of PIJ is its high cost price. Until recently, PIJ print heads were manufactured using bulk $Pb(Zr,Ti)O_3$ (PZT) ceramics as the piezoelectric material in conjunction with micromachining. Scaling up of the thin PZT film deposition process to a 150–200 mm wafer diameter in combination with MEMS processing is a technology enabler for piezo-MEMS print heads with a drastically reduced price. As of today, two companies have introduced printing solutions containing piezo MEMS print heads. Additionally, several companies are considering the application of piezo-MEMS technology for manufacturing piezo-MEMS based print heads for the future.

Hiroshi Funakubo, Interdisciplinary Graduate School of Science and Engineering, Tokyo Institute of Technology; funakubo.h.aa@m.titech.ac.jp
Matthijn Dekkers, SolMateS, The Netherlands
Alessia Sambri, University of Naples Federico II, Italy; sambri@fisica.unina.it
Stefano Gariglio, Condensed Matter Physics Department, University of Geneva; stefano.gariglio@unige.ch
Igor Shklyarevskiy, Oce-Technologies B.V., The Netherlands
Guus Rijnders, University of Twente, The Netherlands; a.j.h.m.rijnders@utwente.nl
DOI: 10.1557/mrs.2012.271

© 2012 Materials Research Society
Downloaded from https://www.cambridge.org/core. University of Basel Library, on 30 May 2017 at 14:40:41, subject to the Cambridge Core terms of use, available at https://www.cambridge.org/core/terms. https://doi.org/10.1557/mrs.2012.271

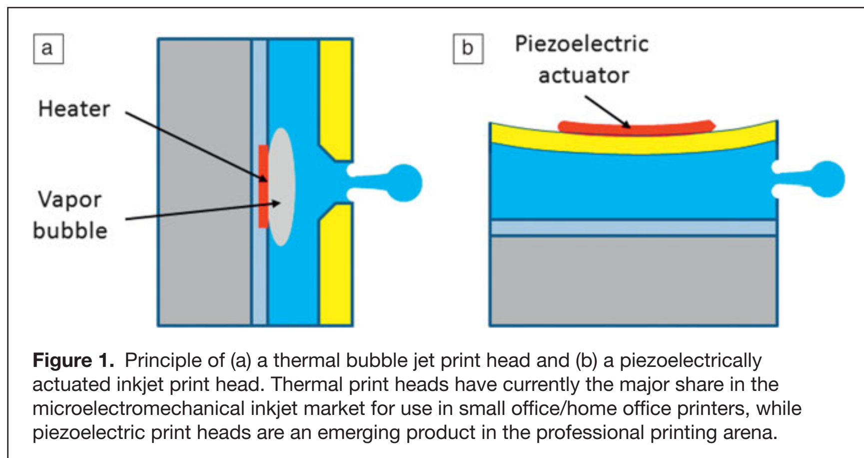

Figure 1. Principle of (a) a thermal bubble jet print head and (b) a piezoelectrically actuated inkjet print head. Thermal print heads have currently the major share in the microelectromechanical inkjet market for use in small office/home office printers, while piezoelectric print heads are an emerging product in the professional printing arena.

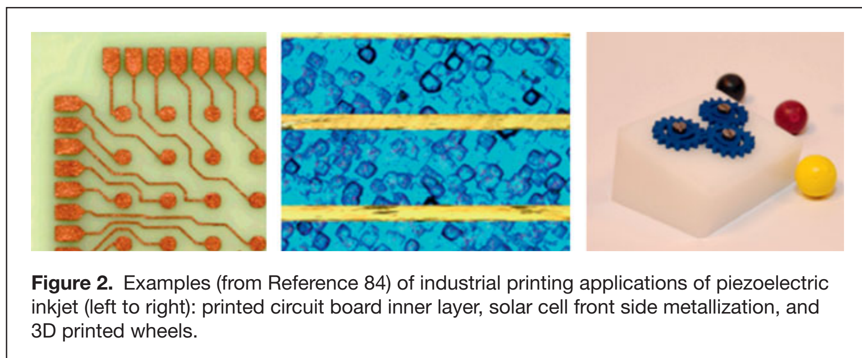

Figure 2. Examples (from Reference 84) of industrial printing applications of piezoelectric inkjet (left to right): printed circuit board inner layer, solar cell front side metallization, and 3D printed wheels.

Although the piezo-MEMS research area is almost two decades old and the integration of thin PZT films in MEMS devices is now an established procedure, reliable operation of such print heads suffers from a combination of several challenging problems, such as actuator stability. Such actuator behavior is the result of instability in the domain state of the film and has a dramatic impact on droplet size and speed during printing, eventually resulting in pixel displacement in the final image. This type of actuator deflection behavior can be explained by the presence of two contributions to the piezoelectric response: intrinsic contributions originating from the stretching/contracting of the unit cell dipoles in the piezoelectric material and extrinsic contributions, mainly attributed to domain wall movement.[4] The deflection decrease was attributed to a change in the domain state, such that after a few actuation cycles, extrinsic contributions and/or re-poling strains no longer contributed.

This effect can be completely eliminated by a thermal poling procedure,[5] which utilizes thermal energy in combination with an electric field to align defect dipole complexes to create an internal electric field aligned with the polarization direction and lock in the domain configuration—an effect known as imprint. It is worthwhile noting that this effect is extremely undesirable in ferroelectric random access memory (FeRAM) devices, while being imperative for proper operation of MEMS actuator devices. Unfortunately, the success of the thermal poling procedure is directly related to the quality and purity of the PZT layer and can be overshadowed by time dependent dielectric breakdown (TDDB) and subsequent catastrophic device failure. Several groups have attributed TDDB to field-driven redistribution of thermally activated oxygen vacancies in the film, resulting in the formation of a forward-biased *p*–*n* junction.[6–8]

There are several methods to reduce the effect of the high defect concentration in PZT films by doping and/or by using oxide electrodes. However, this would only release some pressure on the poling procedure without rendering it unnecessary. Additional progress can be made by removing the poling procedure from the device manufacturing process.

Epitaxial PZT films provide a solution to these issues as, given the right choice of electrodes and deposition method, it can be shown that these films are intrinsically stable without the need for the poling process. In this article, we focus on $Pb(Zr,Ti)O_3$ thin films and in particular on efforts to obtain oriented/epitaxial layers for MEMS applications.

Epitaxial PZT films for MEMS

Among ferroelectric and piezoelectric materials, the perovskite solid solution $Pb(Zr,Ti)O_3$ (PZT) is one of the most prominent compounds given its high electromechanical coupling, large piezoelectric coefficients, and reversible remanent polarization.[9] PZT has piezoelectric coefficients, which relate the mechanical strain produced by an applied electric field or vice versa, that are more than one order of magnitude larger than those of commonly used piezoelectric materials such as ZnO and quartz.[10] The large piezoelectric response for compositions near $Pb(Zr_{0.52}Ti_{0.48})O_3$ rests on the presence of a transition region in the composition phase diagram, called the morphotropic phase boundary,[11] where the crystalline structure changes abruptly. For PZT, this occurs when the tetragonal ferroelectric $PbTiO_3$ mixes in a ~1:1 ratio with the orthorhombic antiferroelectric $PbZrO_3$.[12,13]

In its polycrystalline form, this material is widely used for various applications, such as infrared sensors, ultrasound transducers, and scanning probe tubes.[14,15] In the 1980s, development of thin-film deposition and characterization techniques prompted a technology push for the fabrication of thin-film-based devices, such as FeRAM.[16] In parallel, fundamental understanding of the physical properties of PZT and other ferroelectrics progressed in part as the result of the availability of epitaxial thin films.[17–20]

Epitaxial films provide a well-defined polar axis orientation (see **Figure 3**), as well as high density and compositional uniformity. These are essential to the increases in piezoelectric coefficients.[21] Compared to randomly oriented ceramics, films can be thinner for an equivalent remanent polarization

Downloaded from https:/www.cambridge.org/core. University of Basel Library, on 30 May 2017 at 14:40:41, subject to the Cambridge Core terms of use, available at https:/www.cambridge.org/core/terms. https://doi.org/10.1557/mrs.2012.271

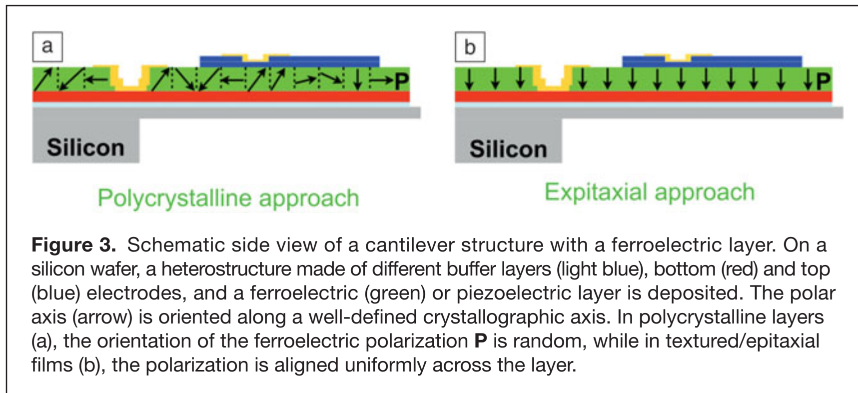

Figure 3. Schematic side view of a cantilever structure with a ferroelectric layer. On a silicon wafer, a heterostructure made of different buffer layers (light blue), bottom (red) and top (blue) electrodes, and a ferroelectric (green) or piezoelectric layer is deposited. The polar axis (arrow) is oriented along a well-defined crystallographic axis. In polycrystalline layers (a), the orientation of the ferroelectric polarization **P** is random, while in textured/epitaxial films (b), the polarization is aligned uniformly across the layer.

while requiring lower coercive voltages, hence lowering the operation voltage. This is certainly a clear advantage for mobile electronics applications such as FeRAMs, where power consumption is an issue.

These advances in thin-film fabrication have motivated the MEMS community to turn to ferroelectrics/piezoelectrics as the transducer layer.[22,23] By utilizing the high piezoelectric response, large-displacement actuators as well as high-sensitivity sensors can be realized. Recently, Baek et al.[24] reported the realization of piezo MEMS based on layers of $Pb(Mg_{1/3}Nb_{2/3})O_3$-$PbTiO_3$, which possesses an extremely high piezoelectric coefficient due to engineered domain states in this relaxor ferroelectric material.

For $x > 0.5$, $Pb(Zr_{1-x}Ti_x)O_3$ is a tetragonal perovskite with the ferroelectric dipole oriented along the long *c*-axis, whereas for $0.1 < x < 0.5$, it becomes rhombohedral. Near the morphotropic phase boundary (MPB) for $x \sim 0.5$, PZT is considered to be monoclinic. This lower symmetry phase acts as a structural bridge between the tetragonal and rhombohedral phases. The electrical and electromechanical properties (piezoelectric coefficients d_{ij}, dielectric constant ε_{ij} where i and j refer to crystallographic orientations for the applied electric field, and the resulting elastic deformation or dielectric response, respectively) are strongly dependent on the orientation of the applied electric field with respect to the crystallographic axes. Hence, the integration of high-quality, highly oriented, and/or epitaxial piezoelectric layers in single-crystal form promises better performance for devices. Moreover, as applications are moving toward smaller, nanoscale devices, such as nanoelectromechanical systems (NEMS), uniformity of the piezoelectric response over nanometer length scales is required. This may limit the use of polycrystalline films due to their microstructural inhomogeneities, which will eventually compromise their performance. The fields of application of this new generation of devices will be sensors (e.g., microbalances), actuators (e.g., piezo-MEMS print heads, piezo cantilevers for atomic force microscopy), and energy harvesters (for the conversion of vibrational energy into electrical energy). Indeed, the development of high-sensitivity mass sensors is in rapid expansion, driven by the quest for the detection of very small masses. High-performance energy harvesting devices have also attracted much interest as small-scale sources of energy capable of powering micro-devices such as wireless sensor networks or monitoring systems for biomedical or environmental applications.[25–33]

Orientation dependence of $Pb(Zr, Ti)O_3$ film properties on single-crystal substrates

The piezoelectric response of oxide crystals is known to depend strongly on their orientation.[34] One straightforward approach to control the orientation of $Pb(Zr,Ti)O_3$ films is their growth on single-crystal substrates with a specific crystalline orientation. In addition, by selecting the lattice constant and thermal expansion coefficient of the substrate, the polar-axis orientation of $Pb(Zr,Ti)O_3$ can be also controlled.[35–37] **Figure 4** shows the orientation dependence of piezoelectric and ferroelectric properties for a series of 2-μm-thick $Pb(Zr_{0.5}Ti_{0.5})O_3$ films prepared by pulsed-metalorganic chemical vapor deposition on (100)-, (110)-, and (111)-oriented $SrTiO_3$ single-crystal substrates buffered with a layer of metallic $SrRuO_3$ used as the bottom electrode.[38] The composition of the films sits at the MPB, and

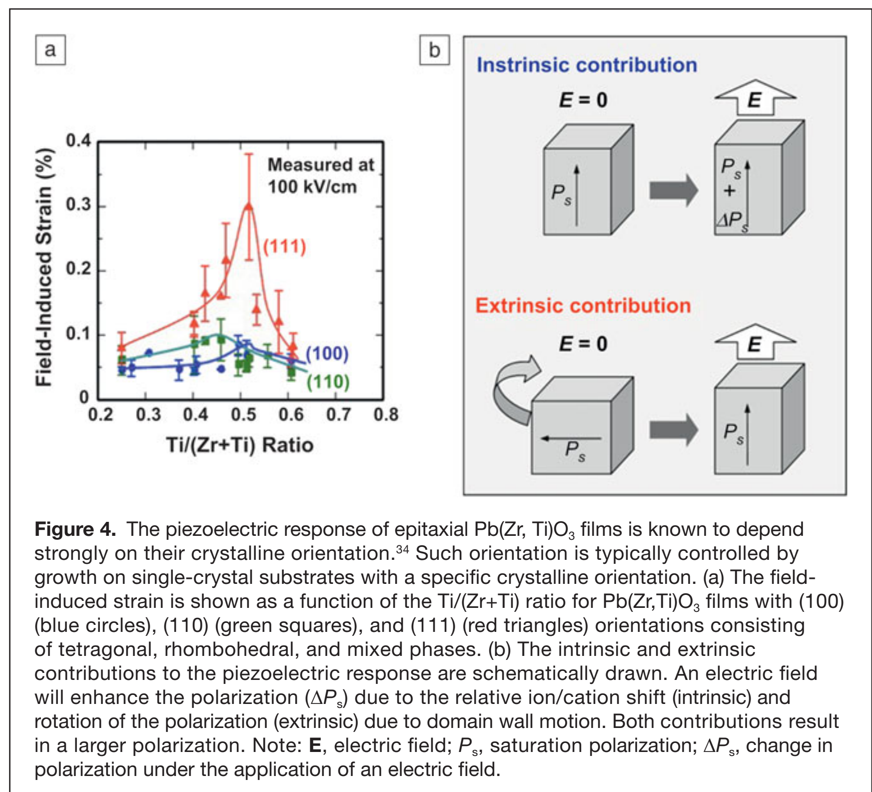

Figure 4. The piezoelectric response of epitaxial $Pb(Zr, Ti)O_3$ films is known to depend strongly on their crystalline orientation.[34] Such orientation is typically controlled by growth on single-crystal substrates with a specific crystalline orientation. (a) The field-induced strain is shown as a function of the Ti/(Zr+Ti) ratio for $Pb(Zr,Ti)O_3$ films with (100) (blue circles), (110) (green squares), and (111) (red triangles) orientations consisting of tetragonal, rhombohedral, and mixed phases. (b) The intrinsic and extrinsic contributions to the piezoelectric response are schematically drawn. An electric field will enhance the polarization (ΔP_s) due to the relative ion/cation shift (intrinsic) and rotation of the polarization (extrinsic) due to domain wall motion. Both contributions result in a larger polarization. Note: **E**, electric field; P_s, saturation polarization; ΔP_s, change in polarization under the application of an electric field.

Downloaded from https://www.cambridge.org/core. University of Basel Library, on 30 May 2017 at 14:40:41, subject to the Cambridge Core terms of use, available at https://www.cambridge.org/core/terms. https://doi.org/10.1557/mrs.2012.271

the resulting phase consists of a mixture of tetragonal and rhombohedral symmetries regardless of the film orientation.[39,40] This coexistence is preserved up to the Curie temperature of about 400°C. Compared to single-phase tetragonal or rhombohedral films, the mixed-phase films show larger orientation dependence of the various properties such as polarization, dielectric constant, and piezoelectric coefficient.

As mentioned previously, the piezoelectric (and dielectric) response in ferroelectrics is due to two contributions:[41] an intrinsic contribution based on the responses of the individual domains, and an extrinsic contribution from domain wall motion (see Figure 4b).[42] For $Pb(Zr,Ti)O_3$, the enhancement of the dielectric and piezoelectric response near the MPB composition can be related to the contribution of not only intrinsic but also extrinsic effects.[43] These data clearly indicate that orientation control is one of the key issues to the realization of a large piezoelectric response in PZT films. It must be noted that which epitaxial orientation is best is currently under investigation because the piezoelectric response of the {100} orientation is larger than that of {111} for fiber textured PZT on Si substrates.[44]

Epitaxial ferroelectric thin films on silicon

As silicon is the modern technological platform for both microelectronic devices and MEMS, a fundamental requirement for the realization of epitaxial piezoelectric MEMS (epi-piezo MEMS) is the integration of the functional piezoelectric layer on silicon wafers. Till the beginning of this century, the availability of epitaxial piezoelectric thin films on silicon has been limited by the hurdles related to the stability of the interface between oxides and silicon.[45] Due to the surface reactivity of silicon, the formation of an amorphous silica layer is a major roadblock to the achievement of a sharp and chemically stable Si/oxide interface. Moreover, the difference in lattice parameters and thermal expansion coefficients between silicon and oxide ferroelectrics represents an extra challenge for the growth of epitaxial thin films. For lead-based ferroelectrics-silicon heterostructures, an additional difficulty derives from Pb cation interdiffusion into the silicon substrate during the growth stage at high temperatures. Such diffusion results in a lead-deficient oxide layer and hence often leads to the formation of pyrochlore/fluorite phases (which are not ferroelectric), with a detrimental effect on the performance of the final devices.[9,46–48]

For these reasons, the strategy for integration of epitaxial ferroelectric thin films on silicon rests on suitable buffer layers that act simultaneously as structural templates and barriers for cation migration.[49–55]

In the late 1980s, different teams actively pursued a process for the deposition of epitaxial oxide layers on Si. Ihara and co-workers[56] investigated the growth of spinel $MgAl_2O_4$ on silicon. Following this work, Matsubara[57] was able to integrate the perovskite $PbTiO_3$ on silicon by using an $MgAl_2O_4$ thin film as a buffer layer. In 1989, the growth of yttria (Y_2O_3) films on Si(100) and of Y_2O_3:ZrO_2 on Si(111) substrates by vacuum evaporation was also demonstrated.[58] This work formed the basis of double buffer layers such as CeO_2/Y_2O_3:ZrO_2 (CeO_2/YSZ). In such stacks, which can be grown by pulsed laser deposition, the YSZ is able to scavenge the native silicon dioxide on the substrate surface,[59] while CeO_2 accommodates the in-plane lattice mismatch with the active ferroelectric perovskite layer. Using these buffer layers, several groups have been able to grow PZT epitaxially on Si.

Yttria-stabilized zirconia/ceria buffer layers

Indeed, yttria-stabilized zirconium oxide (YSZ), with the fluorite crystal structure, grows epitaxially on silicon. With the help of CeO_2 as a second buffer layer, the in-plane epitaxial strain between the YSZ layer and the pseudo-cubic $SrRuO_3$ is reduced to 2.2%, for cube-on-cube growth, if the perovskite cube is rotated by 45° (see **Figure 5**).

It is well-known that the performance of a ferroelectric capacitor is strongly influenced by the electrode material since it affects, among other things, leakage current, dielectric properties, as well as the growth and crystalline structure of ferroelectric films.[60,61] To overcome the problem of fatigue, conducting-oxide electrodes such as RuO_2,[62] $SrRuO_3$ (SRO),[63] $LaNiO_3$,[64] and $(La,Sr)CoO_3$[65] have been used in PZT devices.

Appropriate tailoring of growth conditions can control the crystalline properties of the $SrRuO_3$ electrodes and PZT capacitors. **Figure 6**a shows room-temperature x-ray diffraction (XRD) profiles of PZT/$SrRuO_3$ films on CeO_2/YSZ/Si when $SrRuO_3$ is grown under normal conditions (in this case pulsed laser deposition at 600°C, 13 Pascal). The epitaxial relationship between the buffer layers and silicon is CeO_2(001)‖YSZ(001)‖Si(001), as expected. However, the perovskite layers

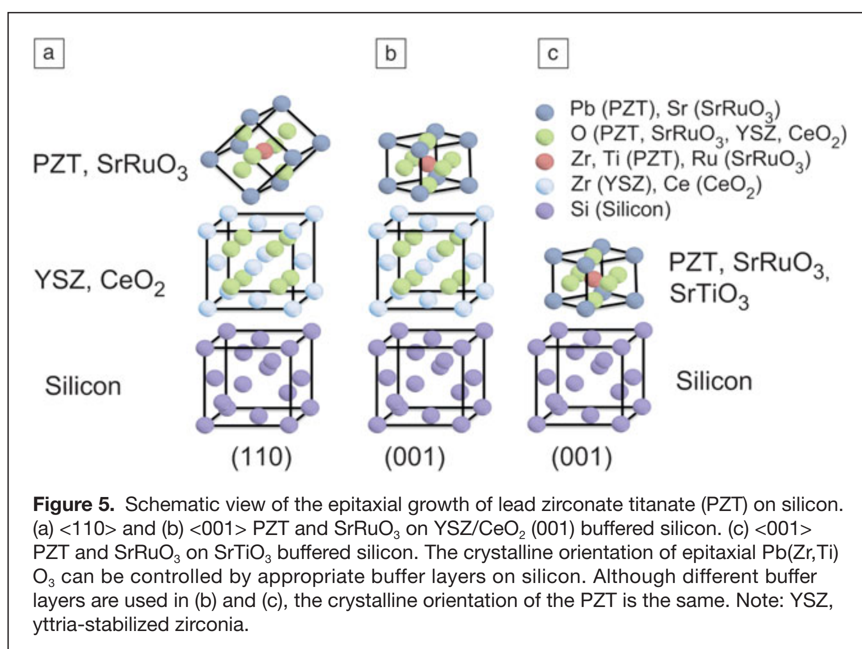

Figure 5. Schematic view of the epitaxial growth of lead zirconate titanate (PZT) on silicon. (a) <110> and (b) <001> PZT and $SrRuO_3$ on YSZ/CeO_2 (001) buffered silicon. (c) <001> PZT and $SrRuO_3$ on $SrTiO_3$ buffered silicon. The crystalline orientation of epitaxial $Pb(Zr,Ti)O_3$ can be controlled by appropriate buffer layers on silicon. Although different buffer layers are used in (b) and (c), the crystalline orientation of the PZT is the same. Note: YSZ, yttria-stabilized zirconia.

Downloaded from https:/www.cambridge.org/core. University of Basel Library, on 30 May 2017 at 14:40:41, subject to the Cambridge Core terms of use, available at https:/www.cambridge.org/core/terms. https://doi.org/10.1557/mrs.2012.271

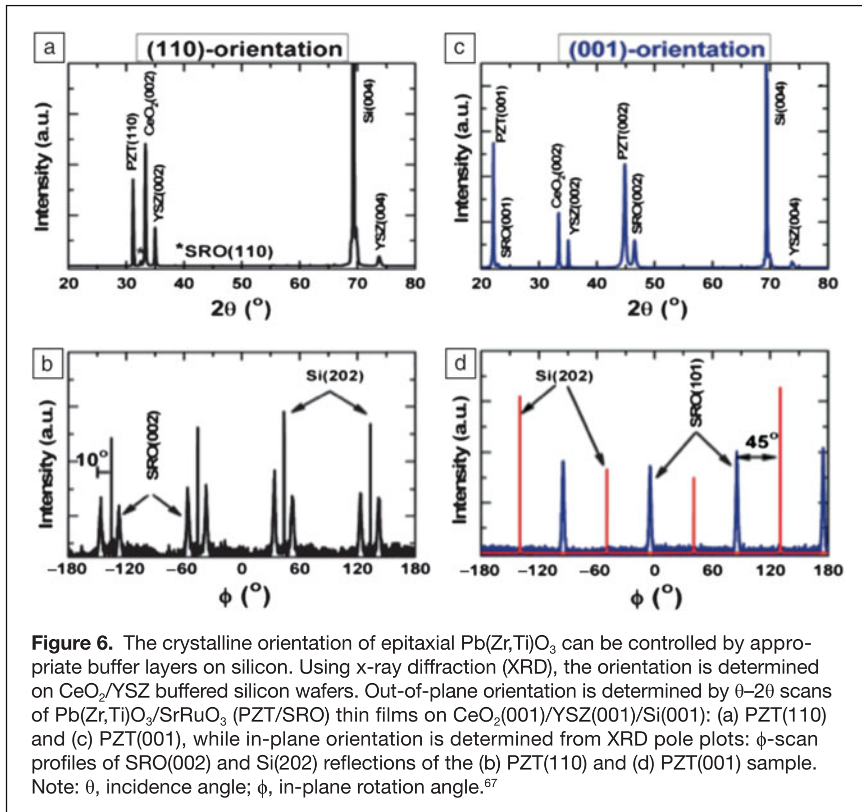

Figure 6. The crystalline orientation of epitaxial Pb(Zr,Ti)O_3 can be controlled by appropriate buffer layers on silicon. Using x-ray diffraction (XRD), the orientation is determined on CeO_2/YSZ buffered silicon wafers. Out-of-plane orientation is determined by θ–2θ scans of Pb(Zr,Ti)O_3/$SrRuO_3$ (PZT/SRO) thin films on CeO_2(001)/YSZ(001)/Si(001): (a) PZT(110) and (c) PZT(001), while in-plane orientation is determined from XRD pole plots: ϕ-scan profiles of SRO(002) and Si(202) reflections of the (b) PZT(110) and (d) PZT(001) sample. Note: θ, incidence angle; ϕ, in-plane rotation angle.[67]

grow (110)-oriented, resulting in the structure PZT(110)‖ $SrRuO_3$(110)‖CeO_2(001)‖YSZ(001)‖Si(001) (as schematically shown in Figure 5a). In-plane XRD analysis of this sample (shown in Figure 6b) reveals four identical sets of two peaks ($SrRuO_3$(002) reflections) positioned around the Si reflections (Si(202) orientation). This indicates that twin domains exist in the thin film.[66] Although CeO_2 is used as a second buffer layer, $SrRuO_3$<111>‖YSZ/Si<110> in-plane epitaxy is still preferred. If a thin $SrRuO_3$ layer (~4 Å, one unit cell) is deposited at a high temperature (800°C) and in a reducing O_2 environment (<10^{-4} Pascal), the epitaxial relation is modified. The deposition conditions favor the re-evaporation of Ru and the formation of a SrO layer, which then acts as a basal plane for the perovskite block. Successive growth of $SrRuO_3$ at 600°C results in (001)-oriented growth of the electrode and the PZT layer, as shown in Figure 6c. The ϕ-scans in Figure 6d reveal a 45° rotation of the $SrRuO_3$(202) orientation compared to the Si(202) orientation. This proves that the unit cells of $SrRuO_3$/PZT are rotated on the CeO_2/YSZ/Si stack, as schematically drawn in Figure 5b.[67]

$SrTiO_3$/SrO as a buffer layer

Driven by the search for high-*k* materials, where *k* is the dielectric constant, for field-effect transistors, a new route for the growth of perovskite layers on silicon was devised in the early 1990s. This solution avoids the formation of amorphous SiO_2 by using alkaline earth metal oxides as buffer layers.[68] Specifically, McKee and co-workers stabilized the interface between silicon and the perovskite layer by the creation of an interfacial silicide layer (BaO, SrO, (Ba, Sr)O) because of the favorable oxidation kinetics of the alkaline earth metals and low temperatures necessary for epitaxial growth.[69] This process, implemented by molecular beam epitaxy (MBE) and assisted by *in situ* monitoring tools, such as reflection high-energy electron diffraction (RHEED), requires a complex multi-step procedure, where fixed amounts of the elemental materials have to be deposited on the silicon substrate.[45,70,71] Starting from $SrTiO_3$-buffered silicon wafers, different groups have reported on the growth of high-quality PZT layers using different deposition techniques.[72,73]

Using radio frequency-magnetron sputter deposition for the growth of $SrRuO_3$/ Pb($Zr_{0.2}Ti_{0.8}O_3$) epitaxial heterostructures on $SrTiO_3$ buffered Si, Sambri et al. reported a remanent polarization of about 70 μC/cm^2, with no significant leakage current up to 16 V and a d_{33} piezoelectric coefficient (this value refers to the geometry where the electric field is applied along the ferroelectric polarization and the displacement is measured along this same axis) from the remanent response, measured by a piezoelectric force microscopy of 50 pm/V for a ferroelectric layer of 100 nm.[74] Here, a 45° rotated cube-on-cube epitaxy of PZT on silicon is found, as schematically depicted in Figure 5c. Using XRD (see **Figure 7**), the following crystallographic relations are estimated: PZT [001]//$SrRuO_3$[001]//$SrTiO_3$[001]//Si[001] (out-of-plane) and PZT[100]//$SrRuO_3$[100]//$SrTiO_3$[100]//Si[110] (in-plane). A 4.5-nm-thick amorphous SiO_2 layer appears at the interface between silicon and $SrTiO_3$ after the growth of the buffer layer and does not affect the epitaxy of the stack, as confirmed by the cross-sectional high-resolution TEM picture in Figure 7.

Role of substrate clamping and strain

Since the PZT film is clamped to the substrate due to the crystalline relationship at the film/substrate interface, the piezoelectric response is influenced by the mechanical boundary conditions, in particular by clamping associated with the thick substrate.[75–77] The difference in crystal lattice parameters and/or the thermal expansion coefficient (TEC) mismatch between the substrate and the clamped thin film upon cooling will result in strain, often referred to as misfit strain (S_M).[78] In epitaxial PZT films much thicker than the critical thickness (>80 nm), the lattice strain is completely relaxed,[79] and the remaining thermal strain is therefore either tensile or compressive depending on the choice of substrate.

Epitaxial Pb($Zr_{0.52}Ti_{0.48}$)O_3 thin-film capacitors with $SrRuO_3$ oxide electrodes[80] on different substrates show substantially different ferroelectric characteristics. **Figure 8**a shows polarization (*P*) measurements as a function of electric field (*E*) (*P-E* loops) of epitaxial (001)-oriented PZT capacitors grown on different substrates. **Table I** shows that the misfit strain for

Downloaded from https://www.cambridge.org/core. University of Basel Library, on 30 May 2017 at 14:40:41, subject to the Cambridge Core terms of use, available at https://www.cambridge.org/core/terms. https://doi.org/10.1557/mrs.2012.271

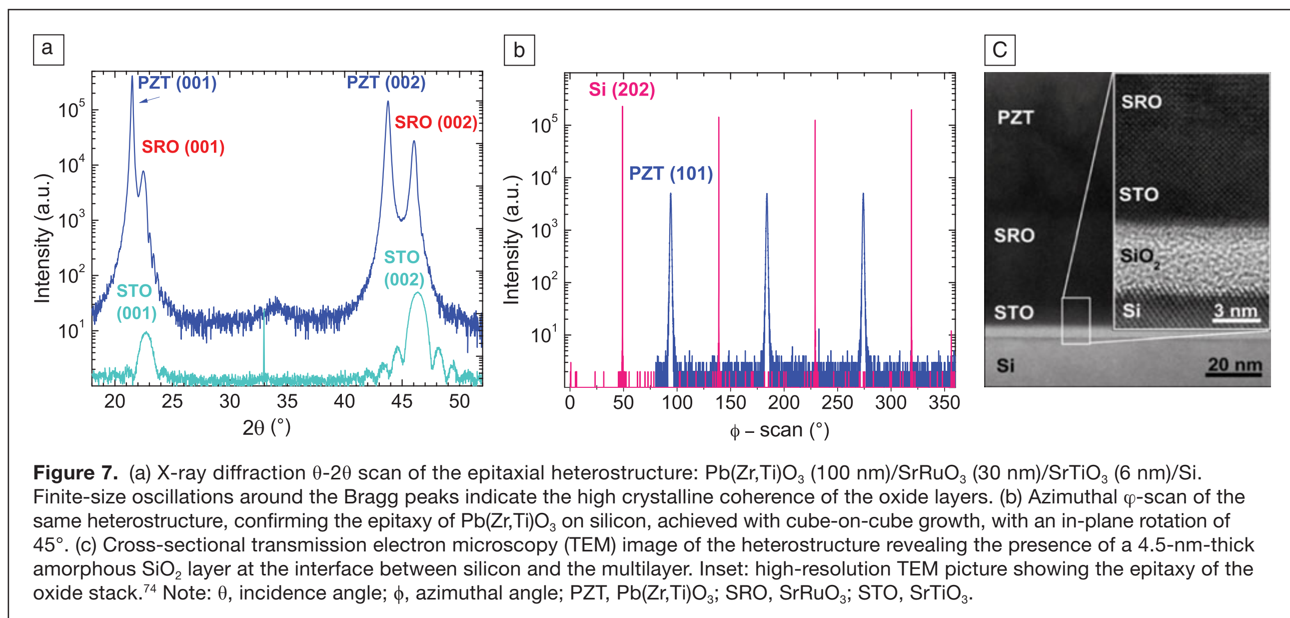

Figure 7. (a) X-ray diffraction θ-2θ scan of the epitaxial heterostructure: $Pb(Zr,Ti)O_3$ (100 nm)/$SrRuO_3$ (30 nm)/$SrTiO_3$ (6 nm)/Si. Finite-size oscillations around the Bragg peaks indicate the high crystalline coherence of the oxide layers. (b) Azimuthal φ-scan of the same heterostructure, confirming the epitaxy of $Pb(Zr,Ti)O_3$ on silicon, achieved with cube-on-cube growth, with an in-plane rotation of 45°. (c) Cross-sectional transmission electron microscopy (TEM) image of the heterostructure revealing the presence of a 4.5-nm-thick amorphous SiO_2 layer at the interface between silicon and the multilayer. Inset: high-resolution TEM picture showing the epitaxy of the oxide stack.[74] Note: θ, incidence angle; ϕ, azimuthal angle; PZT, $Pb(Zr,Ti)O_3$; SRO, $SrRuO_3$; STO, $SrTiO_3$.

these layers ranges from about +2 to -4×10^{-3}. Films on Si substrates are under tensile strain because of the lower TEC of the substrate compared to PZT; conversely, the strain on oxide crystals is compressive due to the higher TEC. It is evident that films with high compressive strain show square and well-saturated hysteresis loops, while the films on silicon have more rounded and slanted hysteresis characteristics. In accordance with theoretical predictions, the average polarization in strained PZT films behaves as if it is neither completely out-of-plane nor completely in-plane.[81] The measured out-of-plane polarization is highest for compressive strain ($S_M < 0$) and lowest for tensile strain ($S_M > 0$). However, whereas the residual polarization P_r decreases, ε_{33} increases as the strain becomes higher.[81] However, the effective piezoelectric response $d_{33,eff}$ is rather independent of strain (Figure 8b).[82] This, of course, is good news for applications, as the actuation and sensing capabilities of PZT in buffered-silicon MEMS are as good as PZT on oxide single crystal substrates.

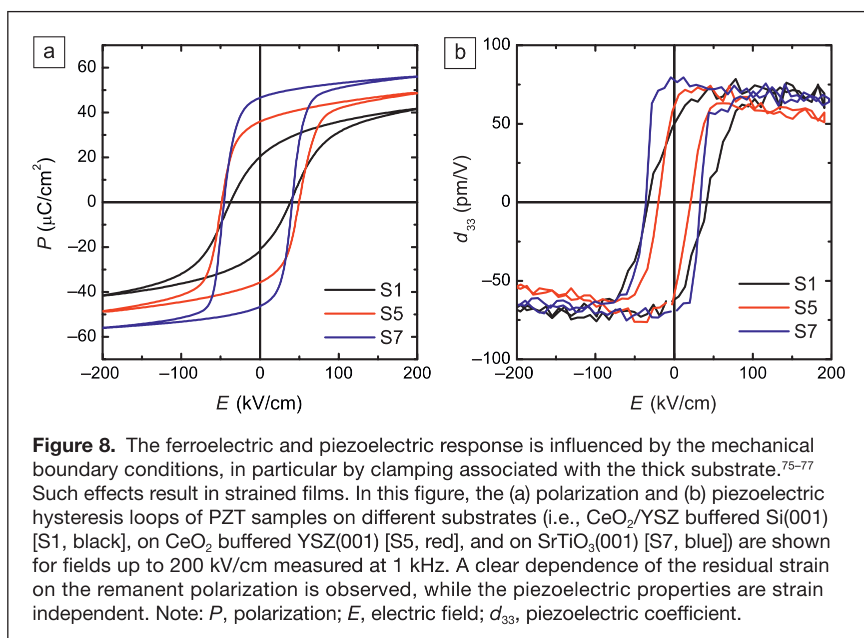

Figure 8. The ferroelectric and piezoelectric response is influenced by the mechanical boundary conditions, in particular by clamping associated with the thick substrate.[75–77] Such effects result in strained films. In this figure, the (a) polarization and (b) piezoelectric hysteresis loops of PZT samples on different substrates (i.e., CeO_2/YSZ buffered Si(001) [S1, black], on CeO_2 buffered YSZ(001) [S5, red], and on $SrTiO_3$(001) [S7, blue]) are shown for fields up to 200 kV/cm measured at 1 kHz. A clear dependence of the residual strain on the remanent polarization is observed, while the piezoelectric properties are strain independent. Note: *P*, polarization; *E*, electric field; d_{33}, piezoelectric coefficient.

Intrinsic stability of PZT properties in relation to crystalline structure

With respect to stability, epitaxial PZT outperforms textured films. Given the right choice of electrodes and deposition method, it is shown that epitaxial films are intrinsically stable. The long-term stability of epitaxial PZT also becomes evident in the actuation of MEMS devices. Silicon-on-insulator (SOI) wafers can be used to deposit epitaxial PZT and processed into MEMS structures. SOI technology refers to a layered silicon-insulator-silicon substrate in place of conventional silicon substrates, which are used in, for instance, microelectronics, to reduce parasitic device capacitance. SOI technology is also widely used in the fabrication of MEMS devices, where the top Si layer is typically used as the device layer, and the SiO_x insulator as the etch stopping layer. Since the top Si layer is single crystalline with a perfect controlled orientation, epitaxial growth of PZT using the previously mentioned buffer layers can be reproducibly achieved. **Figure 9**a–d shows a typical process flow of the fabrication of membranes and cantilevers using wet chemical and dry etching techniques. Fabricated cantilevers show no fatigue and stable displacement for up to 10^{10} actuation cycles, as observed in Figure 9e.[83]

Summary

We have reported on progress in lead zirconate titanate (PZT) thin-film deposition processes,

Downloaded from https:/www.cambridge.org/core. University of Basel Library, on 30 May 2017 at 14:40:41, subject to the Cambridge Core terms of use, available at https:/www.cambridge.org/core/terms. https://doi.org/10.1557/mrs.2012.271

Table I. Measured and calculated properties of lead zirconate titanate (PZT) samples on different substrates in the order of decreasing misfit strain.[82]

Buffer/Substrate	a	c	S_M	TEC	P_r	P_s	ε_{33}	Max d_{33eff}
	(Å)	(Å)	(10^{-3})	(10^{-6} K^{-1})	(μC/cm^2)	(μC/cm^2)		(pm/V)
CeO_2/YSZ/Si	4.108	4.087	1.71	2.6	20.9	31.4	378	72.8
$SrTiO_3$/Si	4.088	4.080	0.65	2.6	27.3	34.3	260	74.2
CeO_2/YSZ	4.062	4.092	–2.45	11.4	35.8	40.4	184	74.4
$SrTiO_3$	4.061	4.113	–4.23	11.0	46.5	50.5	165	75.2

a (Å) and c (Å), in-plane and out-of-plane lattice constants, respectively; S_M, misfit strain; TEC, thermal expansion coefficient of the substrate; P_r, out-of-plane polarization; P_s, saturation polarization; ε_{33}, dielectric constant; and $d_{33,eff}$, effective piezoelectric response. Note: YSZ, yttria-stabilized zirconia.

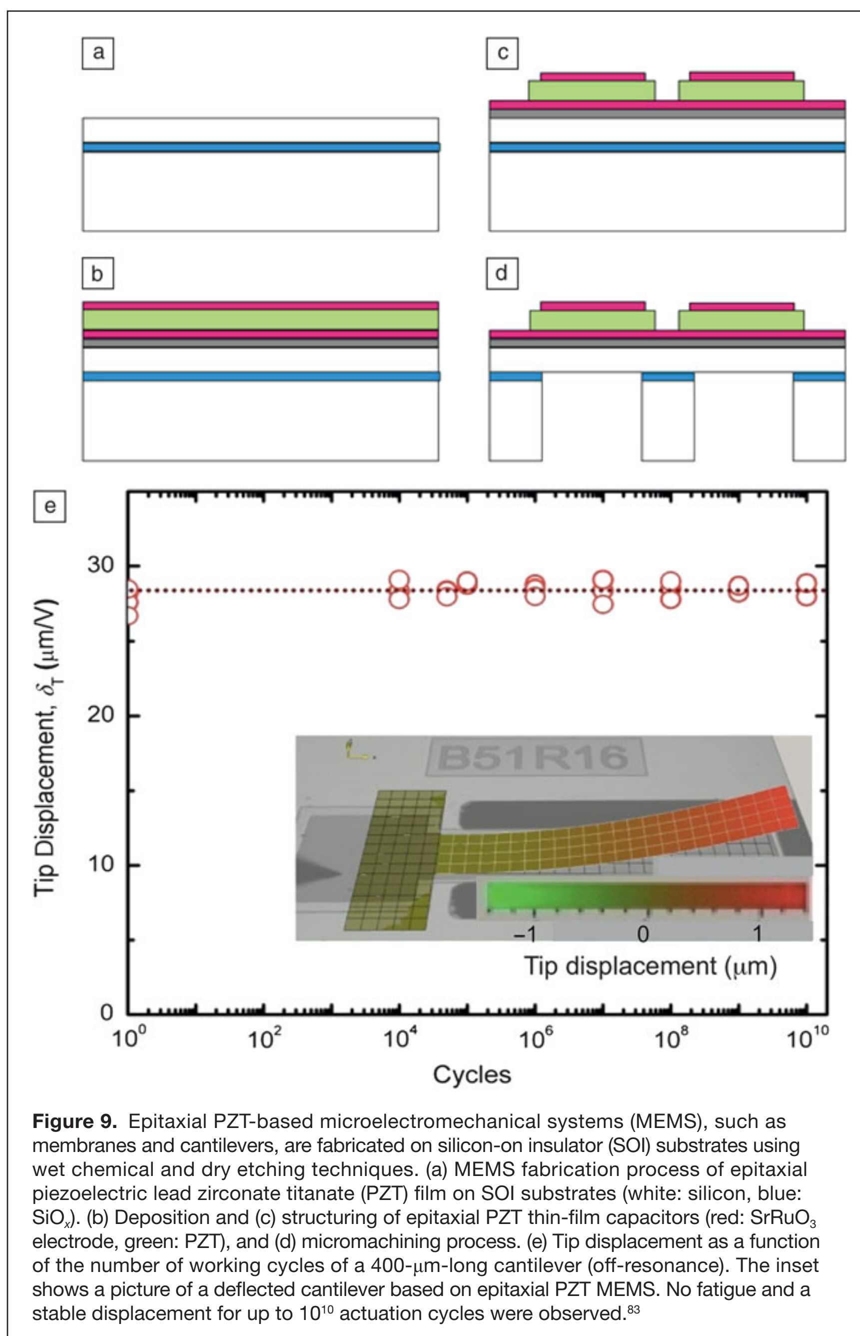

Figure 9. Epitaxial PZT-based microelectromechanical systems (MEMS), such as membranes and cantilevers, are fabricated on silicon-on insulator (SOI) substrates using wet chemical and dry etching techniques. (a) MEMS fabrication process of epitaxial piezoelectric lead zirconate titanate (PZT) film on SOI substrates (white: silicon, blue: SiO_x). (b) Deposition and (c) structuring of epitaxial PZT thin-film capacitors (red: $SrRuO_3$ electrode, green: PZT), and (d) micromachining process. (e) Tip displacement as a function of the number of working cycles of a 400-μm-long cantilever (off-resonance). The inset shows a picture of a deflected cantilever based on epitaxial PZT MEMS. No fatigue and a stable displacement for up to 10^{10} actuation cycles were observed.[83]

which allow control of the crystalline orientation of oxide epitaxial heterostructures on silicon. For piezoelectric layers, this approach enables orienting the polar axis in a well-defined direction to maximize the electromechanical response. Ferroelectric and mechanical measurements of epitaxial PZT-based microelectromechanical systems (MEMS) show the potential of this approach: poling is no longer needed, and fatigue is strongly suppressed. Such epitaxial piezoelectric layers integrated in MEMS show enhanced performance and will enable reliable and stable operation in near-future piezo print heads.

Although the inkjet printing industry is maturing for PZT-based MEMS technology, current piezoelectric PZT thin-film technology and the use of "traditional" electrode materials such as Pt are already known to impair performance on the industrial scale, demanding novel material solutions, such as the use of epitaxial PZT thin films and epitaxial (oxide) electrode materials. Further developments, such as miniaturization down to the sub-micron scale, will put even tighter constraints on materials and processing, demanding new approaches and concepts. The rich variety of properties offered by epitaxial PZT will provide viable solutions as well as promising new functionalities. To achieve this, knowledge and know-how transfer of epitaxial PZT-based MEMS structures from basic research to industrial applications is required. This includes development of novel industrial scale fabrication processes for epitaxial PZT films and MEMS devices on industrial scale Si and silicon-on-insulator wafers (up to 200 mm).

Acknowledgments

H.F. acknowledges a grant from the Japan Society for the Promotion of Science (JSPS) through the Funding Program for World-Leading Innovative R&D on Science and Technology

Downloaded from https://www.cambridge.org/core. University of Basel Library, on 30 May 2017 at 14:40:41, subject to the Cambridge Core terms of use, available at https://www.cambridge.org/core/terms. https://doi.org/10.1557/mrs.2012.271

(FIRST Program), initiated by the Council for Science and Technology Policy (CSTP) and Ministry of Education, Culture, Sports, Science and Technology of Japan. T.Y. acknowledges a grant from the Japan Science and Technology Agency (JST) through the Precursory Research for Embryonic Science and Technology (PRESTO) program. A.S. and S.G. acknowledge support from the Swiss National Science Foundation through the National Center of Competence in Research "Materials with Novel Electronic Properties-MaNEP" and the EU Project Oxides. Discussions with P. Zubko are gratefully acknowledged. G.R., M.D., and I.S. acknowledge support from the Dutch government through the SmartMix programme. Discussions with M. Nguyen, E. Houwman, R. Steenwelle, and X. Wan are gratefully acknowledged.

References

1. "Status of the MEMS industry" (Market and Technology Report, Yole Development, Rockville, MD, July 2011).
2. M.A. Groninger, P.G.M. Kruijt, H. Reinten, R.H. Schippers, J.M.M. Simons, European Patent EP 1 378 360 A1 (2003).
3. K.S. Kwon, W. Kim, *Sens. Actuators, A* **140**, 75 (2007).
4. D. Damjanovic, *J. Am. Ceram. Soc.* **88** (10), 2663 (2005).
5. M. Kohli, A. Seifert, P. Muralt, *Integr. Ferroelectr.* **22** (1), 453 (1998).
6. S.B. Desu, I.K. Yoo, *J. Electrochem. Soc.* **140**, L133 (1993).
7. D.J. Wouters, G. Willems, G. Groeseneken, H.E. Meas, K. Brooks, *Integr. Ferroelectr.* **7**, 173 (1995).
8. T. Baiatu, R. Waser, K.-H. Hardtl, *J. Am. Ceram. Soc.* **73**, 1663 (1990).
9. G. Shirane, K. Suzuki, *J. Phys. Soc. Jpn.* **7**, 333 (1952).
10. D.L. Polla, L.F. Francis, *Annu. Rev. Mater. Sci.* **28**, 563 (1998).
11. B. Jaffe, R.S. Roth, S. Marzullo, *J. Appl. Phys.* **25**, 809 (1954).
12. B. Noheda, D.E. Cox, G. Shirane, J.A. Gonzalo, L.E. Cross, S.-E. Park, *Appl. Phys. Lett.* **74**, 2059 (1999).
13. R. Guo, L.E. Cross, S.-E. Park, B. Noheda, D.E. Cox, G. Shirane, *Phys. Rev. Lett.* **84**, 5423 (2000).
14. R.W. Schwartz, J. Ballato, G.H. Heartling, in *Ceramic Materials for Electronics*, R.C. Buchanan, Ed. (Marcel Dekker, New York, 2004), pp. 207–322.
15. R. Takayama, Y. Tomita, *J. Appl. Phys.* **65**, 1666 (1989).
16. J. Scott, C. Araujo, *Science* **246**, 1400 (1989).
17. T. Tybell, C.H. Ahn, J.-M. Triscone, *Appl. Phys. Lett.* **75**, 856 (1999).
18. D. Fong, G. Stephenson, S. Streiffer, J. Eastman, O. Auciello, P. Fuoss, C. Thompson, *Science* **304**, 1650 (2004).
19. H. Morioka, G. Asano, T. Oikawa, H. Funakubo, K. Saito, *Appl. Phys. Lett.* **82**, 4761 (2003).
20. I. Vrejoiu, G. Le Rhun, L. Pintilie, D. Hesse, M. Alexe, U. Gosele, *Adv. Mater.* **18**, 1657 (2006).
21. P. Muralt, R. Polcawich, S. Trolier-Mckinstry, *MRS Bull.* **34**, 658 (2009).
22. S. Trolier-McKinstry, P. Muralt, *J. Electroceram.* **12**, 7 (2004).
23. P. Muralt, *J. Am. Ceram. Soc.* **91**, 1385 (2008).
24. S.H. Baek, J. Park, D.M. Kim, V. Aksyuk, R.R. Das, S.D. Bu, D.A. Felker, J. Lettieri, V. Vaithyanathan, S.S.N. Bharadwaja, N. Bassiri-Gharb, Y.B. Chen, H.P. Sun, C.M. Folkman, H.W. Jang, D.J. Kreft, S.K. Streiffer, R. Ramesh, X.Q. Pan, S. Trolier-McKinstry, D.G. Schlom, M.S. Rzchowski, R.H. Blick, C.B. Eom, *Science* **334**, 958 (2011).
25. Y.B. Jeon, R. Sood, J.-H. Jeong, S.-G. Kim, *Sens. Actuators, A* **122**, 16 (2005).
26. S. Roundy, P.K. Wright, *Smart Mater. Struct.* **13** 1131 (2004).
27. H.-C. Song, H.-C. Kim, C.-Y. Kang, H.-J. Kim, S.-J. Yoon, D.-Y. Jeong, *J. Electroceram.* **23**, 301 (2009).
28. H.-B. Fang, J.-Q. Liu, Z.-Y. Xu, L. Dong, L. Wang, D. Chen, B.-C. Cai, Y. Liu, *Microelectron. J.* **37**, 1280 (2006).
29. D. Shen, J.-H. Park, J. Ajitsaria, S.-Y. Choe, H.C. Wikle, D.-J. Kim, *J. Micromech. Microeng.* **18**, 055017 (2008).
30. T. Xu, Z. Wang, J. Miao, L. Yu, C.M. Li, *Biosens. Bioelectron.* **24**, 638 (2008).
31. J.Z. Tsai, C.J. Chen, W.Y. Chen, J.T. Liu, C.Y. Liao, Y.M. Hsin, *Sens. Actuators, B* **139**, 259 (2009).
32. W. Pang, L. Yan, H. Zhang, H. Yu, E.S. Kim, W.C. Tang, *Appl. Phys. Lett.* **88**, 243503 (2006).
33. S. Shin, N.-E. Lee, H.-D. Park, J.-S. Park, J. Lee, *Integr. Ferroelectr.* **80**, 355 (2006).
34. S.E. Park, T.R. Shrout, *J. Appl. Phys.* **82**, 1804 (1997).
35. S. Utsugi, T. Fujisawa, R. Ikariyama, S. Yasui, H. Nakaki, T. Yamada, M. Ishikawa, M. Matsushima, H. Morioka, H. Funakubo, *Appl. Phys. Lett.* **94**, 052906 (2009).
36. T. Fujisawa, H. Nakaki, R. Ikariyama, T. Yamada, H. Funakubo, *Appl. Phys. Express* **1**, 085001 (2008).
37. S. Utsugi, T. Fujisawa, Y. Ehara, T. Yamada, M. Matsushima, H. Funakubo, *Appl. Phys. Lett.* **96**, 102905 (2010).
38. C.B. Eom, R.J. Cava, R.M. Fleming, J.M. Phillips, R.B. van Dover, J.H. Marshall, J.W.P. Hsu, J.J. Krajewski, W.F. Peck Jr., *Science* **258**, 1799 (1992).
39. S. Yokoyama, Y. Honda, H. Morioka, T. Oikawa, H. Funakubo, T. Iijima, H. Matsuda, K. Saito, *Appl. Phys. Lett.* **83**, 2408 (2003).
40. S. Yokoyama, Y. Honda, H. Morioka, S. Okamoto, H. Funakubo, T. Iijima, H. Matsuda, K. Saito, T. Yamamoto, H. Okino, O. Sakata, S. Kimura, *J. Appl. Phys.* **98**, 94106 (2005).
41. L.E. Cross, *Mater. Chem. Phys.* **43**, 108 (1996).
42. H. Fu, R.E. Cohen, *Nature* **403**, 281 (2000).
43. D.-J. Kim, J. Maria, A.I. Kingon, S.K. Streiffer, *J. Appl. Phys.* **93**, 5568 (2003).
44. P. Muralt, *J. Amer. Ceram. Soc.* **91**, 1385 (2008).
45. J.W. Reiner, A.M. Kolpak, Y. Segal, K.F. Garrity, S. Ismail-Beigi, C.H. Ahn, F.J. Walker, *Adv. Mater.* **22**, 2919 (2010).
46. D.S. Shin, S.T. Park, H.S. Choi, I.H. Choi, J.Y. Lee, *Thin Solid Films* **354**, 251 (1999).
47. E. Tokumitsu, K. Itani, B.-K. Moon, H. Ishiwara, *Jpn. J. Appl. Phys.* **34**, 5202 (1995).
48. P. Revesz, J. Li, N. Szabo Jr., W. Mayer, D. Caudillo, E.R. Myers, *Mater. Res. Soc. Symp. Proc.* **243**, 101 (1991).
49. A.K. Sharma, J. Narayan, C. Jin, A. Kvit, S. Chattopadhyay, C. Lee, *Appl. Phys. Lett.* **76**, 1458 (2000).
50. M.B. Lee, M. Kawasaki, M. Yoshimoto, H. Koinuma, *Jpn. J. Appl. Phys.* **35**, L574 (1996).
51. N.A. Basit, H.K. Kim, J. Blachere, *Appl. Phys. Lett.* **73**, 3941 (1998).
52. Y. Wang, C. Ganpule, B.T. Liu, H. Li, K. Mori, B. Hill, M. Wuttig, R. Ramesh, *Appl. Phys. Lett.* **80**, 97 (2002).
53. Y.K. Wang, T.Y. Tseng, P. Lin, *Appl. Phys. Lett.* **80**, 3790 (2002).
54. B.T. Liu, K. Maki, Y. So, V. Nagarajan, R. Ramesh, J. Lettieri, J.H. Haeni, D.G. Schlom, W. Tian, X.Q. Pan, F.J. Walker, R.A. McKee, *Appl. Phys. Lett.* **80**, 4801 (2002).
55. B.K. Moona, H. Ishiwaraa, E. Tokumitsua, M. Yoshimoto, *Thin Solid Films* **385**, 307 (2001).
56. M. Ihara, Y. Arimoto, M. Jifuku, T. Kimura, S. Kodama, H. Yamawaki, T. Yamaoka, *J. Electrochem. Soc.* **129**, 2569 (1982).
57. S. Matsubara, *Jpn. J. Appl. Phys.* **24**, 10 (1985).
58. H. Fukumoto, H. Fukumoto, T. Imura, Y. Osaka, *Appl. Phys. Lett.* **55**, 360 (1989).
59. S.J. Wang, C.K. Ong, L.P. You, S.Y. Xu, *Semicond. Sci. Technol.* **15**, 836 (2000).
60. J.J. Lee, C.L. Thio, S.B. Desu, *J. Appl. Phys.* **78**, 5073 (1995).
61. A.Q. Jiang, J.F. Scott, M. Dawber, C. Wang, *J. Appl. Phys.* **92**, 6756 (2002).
62. C.W. Law, K.Y. Tong, J.H. Li, K. Li, M.C. Poon, *Thin Solid Films* **354**, 162 (1999).
63. C.B. Eom, R.B. van Dover, J.M. Phillips, D.J. Werder, J.H. Marshall, C.H. Chen, R.J. Cava, R.M. Fleming, D.K. Fork, *Appl. Phys. Lett.* **63**, 2570 (1993).
64. M-.S. Chen, T.-B. Wu, J.-M. Wu, *Appl. Phys. Lett.* **68**, 1430 (1996).
65. J. Lee, C.H. Choi, B.H. Park, T.W. Noh, J.K. Lee, *Appl. Phys. Lett.* **72**, 3380 (1998).
66. S.Y. Hou, J. Kwo, R.K. Watts, J.-Y. Cheng, D.K. Fork, *Appl. Phys. Lett.* **67**, 1387 (1995).
67. M. Dekkers, M.D. Nguyen, R. Steenwelle, P.M. te Riele, D.H.A. Blank, G. Rijnders, *Appl. Phys. Lett.* **95**, 012902 (2009).
68. H. Mori, H. Ishiwara, *Jpn. J. Appl. Phys.* **30**, L1415 (1991); R.A. McKee, F.J. Walker, J.R. Conner, E.D. Specht, D.E. Zelmon, *Appl. Phys. Lett.* **59**, 782 (1991); R.A. McKee, F.J. Walker, M.F. Chisholm, *Phys. Rev. Lett.* **81**, 3014 (1998).
69. K.J. Hubbard, D.G. Schlom, *J. Mater. Res.* **11**, 2757 (1996); D.G. Schlom, J.H. Haeni, *Mat. Res. Bull.* **27**, 198 (2002).
70. J. Lettieri, J.H. Haeni, D.G. Schlom, *J. Vac. Sci. Technol., A* **20**, 1332 (2002).
71. J.W. Reiner, K.F. Garrity, F.J. Walker, S. Ismail-Beigi, C.H. Ahn, *Phys. Rev. Lett.* **101**, 105503 (2008).
72. A. Lin, X. Hong, V. Wood, A.A. Verevkin, C.H. Ahn, R.A. McKee, F.J. Walker, E.D. Specht, *Appl. Phys. Lett.* **78**, 2034 (2001).
73. D.M. Kim, C.B. Eom, V. Nagarajan, J. Ouyang, R. Ramesh, V. Vaithyanathan, D.G. Schlom, *Appl. Phys. Lett.* **88**, 142904 (2006).
74. A. Sambri, S. Gariglio, A. Torres Pardo, J.-M. Triscone, O. Stéphan, J.W. Reiner, C.H. Ahn, *Appl. Phys. Lett.* **98**, 12903 (2011).

Downloaded from https://www.cambridge.org/core. University of Basel Library, on 30 May 2017 at 14:40:41, subject to the Cambridge Core terms of use, available at https://www.cambridge.org/core/terms. https://doi.org/10.1557/mrs.2012.271

75. J. Ouyang, R. Ramesh, A.L. Roytburd, *Appl. Phys. Lett.* **86**, 152901 (2005).
76. D.M. Kim, C.-B. Eom, V. Nagarajan, J. Ouyang, R. Ramesh, V. Vaithyanathan, D.G. Schlom, *Appl. Phys. Lett.* **88**, 142904 (2006).
77. J. Pérez de la Cruz, E. Joanni, P.M. Vilarinho, A.L. Kholkin, *J. Appl. Phys.* **108**, 114106 (2010).
78. P.-E. Janolin, *J. Mater. Sci.* **44**, 5025 (2009).
79. S. Gariglio, N. Stucki, J.-M. Triscone, G. Triscone, *Appl. Phys. Lett.* **90**, 202905 (2007).
80. C.B. Eom, R.J. Cava, R.M. Fleming, J.M. Phillips, R.B. van Dover, J.H. Marshall, J.W.P. Hsu, J.J. Krajewski, W.F. Peck Jr., *Science* **258**, 1799 (1992).
81. N.A. Pertsev, V.G. Kukhar, H. Kohlstedt, R. Waser, *Phys. Rev. B.* **67**, 054107 (2003).
82. M.D. Nguyen, M. Dekkers, E. Houwman, R. Steenwelle, X. Wan, A. Roelofs, T. Schmitz-Kempen, G. Rijnders, *Appl. Phys. Lett.* **99**, 252904 (2011).
83. M.D. Nguyen, H. Nazeer, K. Karakaya, S.V. Pham, R. Steenwelle, M. Dekkers, L. Abelmann, D.H.A. Blank, G. Rijnders, *J. Micromech. Microeng.* **20**, 085022 (2010).
84. E . van Genuchten, *Mikroniek* **1**, 5 (2011).

materials360 online
your premier source for materials science news
www.materials360online.com
Home | News | About | Publications

Your Search Stops Here!

- Breaking Research News
- MRS News
- Hot Topics
- Featured Journal Articles
- Videos and Podcasts
- Education and Outreach Links
- Twitter Feeds
- And More

INTRODUCING MATERIALS360 ONLINE

The Materials Research Society (MRS) and Cambridge University Press proudly announce the launch of a new website dedicated to materials science news, ***Materials360 Online.***

Materials360 Online features original news stories, videos and podcasts reported and written by MRS staff, volunteers and freelancers. The site also brings you news stories aggregated from many other major scientific publications and websites, so you won't have to search anywhere else for your materials news. The search stops here! Visit regularly and don't miss a single day's worth of valuable news and information.

Downloaded from https://www.cambridge.org/core. University of Basel Library, on 30 May 2017 at 14:40:41, subject to the Cambridge Core terms of use, available at https://www.cambridge.org/core/terms. https://doi.org/10.1557/mrs.2012.271